Available online at www.sciencedirect.com
ScienceDirect
Journal of Power Sources 174 (2007) 2–8
JOURNAL OF POWER SOURCES
www.elsevier.com/locate/jpowsour

Electrochemical characterization of high-power lithium ion batteries using triangular voltage and current excitation sources

Mark W. Verbrugge [a,*], Ping Liu [b]

[a] *General Motors Corporation, Materials & Processes Lab, R&D Center, 30500 Mound Road, Mail Code 480 106 224, P.O. Box 9055, Warren, MI 48090-9055, United States*
[b] *HRL Laboratories, LLC, 3011 Malibu Canyon Road, Malibu, CA 90265, United States*

Received 12 February 2007; received in revised form 11 March 2007; accepted 12 March 2007
Available online 16 March 2007

Abstract

We derive and implement analytic solutions for the description of batteries subject to cyclic voltage and current sources of varying amplitudes, consistent with vehicle drive events. An equivalent circuit comprising a resistor in series with a parallel resistor–capacitor combination is employed. The method we develop is applied to a high-power lithium ion cell, thereby allowing us to obtain parameters and overall characteristics useful for (1) representing the battery in system (e.g., vehicle) models and (2) providing a quantitative means of comparing and classifying battery systems. Closed-form analytic solutions derived using Fourier series are compared with experimental data.

Keywords: Battery; Cyclic voltammetry; Chronopotentiometry; Equivalent circuit; Lithium titanate

1. Introduction

To facilitate the integration of traction batteries within vehicle systems, procedures must be developed to characterize the devices and extract relevant parameters. The control algorithms employed in hybrid electric vehicles (HEVs) rely on simplified models that are linear and admit rapid calculation, commensurate with robust vehicle operation and embedded controller capabilities (execution times and storage). Such control algorithms are used to determine the state of charge, state of health, and power capability of the energy storage system [1–5]. The United States Advanced Battery Consortium, in conjunction with the FreedomCAR initiative, has provided target specifications for HEV batteries and associated test procedures [6]. The test procedures, however, do not lend themselves to the straightforward determination of the parameters associated with the equivalent circuit depicted in Fig. 1, which is often used to correlate battery performance and is used by many automakers (including GM) to represent battery systems in full vehicle modeling. The parameters R, R_{ct}, and C are expected to vary with temperature and SOC, and a method to assess such variations is needed.

By controlling the cell potential (and enforcing current limits), one can ensure that the cell state is well controlled during the test conditions. Cyclic voltammetry [7], wherein the cell potential is changed linearly with time, renders an easily implemented and interpreted procedure for analysis. There are also times when electrochemical systems are best analyzed using a triangular current sweep excitation source [7], particularly when one wants to avoid high current passage. In this work we provide analytic expressions for cyclic voltammetry and triangular current sweep chronopotentiometry of electrochemical cells that can be represented by the equivalent circuit depicted in Fig. 1. An analogous approach was recently presented by the authors for supercapacitor cells [8]. In that case, a series RC circuit was employed; i.e., R_{ct} infinite in Fig. 1. All formulae derived in this work for cyclic voltammetry transform to those of Ref. [8] when R_{ct} is taken to be infinite.

When developing an approximate model for a complicated system, one must ask "can the data be well represented by the model if the model parameters are held constant?" If the model cannot correlate a broad range of data with sufficient accuracy, then additional complexity must be incorporated within the model representation. We include a number of

* Corresponding author. Tel.: +1 586 986 2010; fax: +1 586 986 3091.
E-mail address: mark.w.verbrugge@gm.com (M.W. Verbrugge).

0378-7753/$ – see front matter © 2007 Elsevier B.V. All rights reserved.
doi:10.1016/j.jpowsour.2007.03.019

Nomenclature

C	capacitance (F)
F	Faraday's constant (96,487 C mol^{-1})
I	current (A)
Q	charge on the capacitor (C)
r	R/R_{ct}
R	high-frequency resistance (Ω)
R_{ct}	Effective interfacial resistance (Ω)
R_g	gas constant (8.314 J mol^{-1} K)
SOC	percent state of charge (energy content in the battery relative to the energy content upon full charge)
t	time (s)
T	temperature (K)
U^o	defined in Eq. (1)
V	cell voltage (V)
V_0	open-circuit voltage (V)

Greek letters

α	RC/θ
ν	frequency of excitation source (s^{-1})
θ	half-cycle duration (s)
τ	t/θ

experiment–theory comparisons over a broad range of operating conditions using the same set of parameter values in this work. An important implication associated with the successful comparison of the analytic solutions with experimental data is that control algorithms based on the equivalent circuit of Fig. 1 can be expected to work well in terms of correlating (adaptively) the performance of the battery system. While the algorithms can be implemented to regress adaptively the parameter values during vehicle operation, it is necessary to place bounds on the adapted parameters for robust operation [9–18], and the base parameter values are also required to assess the state of health of the battery. In a related vein, we note that several researchers have attempted to infer the SOC by first correlating the equivalent circuit parameter values as a function of SOC and then measuring the parameter values (e.g., by ac impedance methods) of the battery in different states [19–25].

The intention of the simplified model presented in this work is to provide rapid parameter identification of battery systems. No details about the underlying electrode morphology are involved. While an obvious weakness of this approach is that it cannot be used to design improved electrodes in an explicit manner, a corresponding strength is that detailed knowledge of the cell electrochemistry is not required. We shall not comment further on the detailed characteristics of the cell investigated other than to note that it is representative of batteries comprising a lithium titanate anode and cobalt oxide cathode.

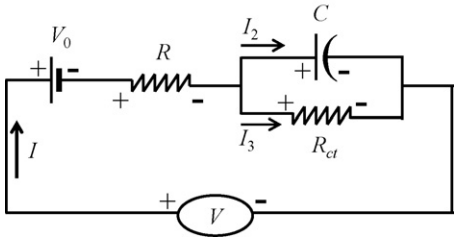

Fig. 1. Equivalent circuit for correlating the cell behavior. Positive currents denote battery charging.

This paper is organized as follows. After describing the experimental elements of this work, we derive the mathematical relations employed to simulate voltammetric and chronopotentiometric operation of battery cells. The following section provides a discussion of results, including the comparison of closed-form analytic solutions with experimental data. We close with a short summary and a description of open questions and remaining challenges.

2. Experimental

Over the voltage range of 1.8–2.8 V, the prismatic cells maintain a capacity of approximately 2.7 Ah. Prior to each of the cyclic voltammetry tests, the cell was charged at the $C/10$ rate (0.27 A) to 2.8 V, held at that voltage until the current dropped to less than 50 mA, and subsequently discharged at a $C/10$ rate for 2, 4, 6, or 8 h to reach depths of discharge (DOD) of 20, 40, 60, or 80%, respectively. The cell was placed in the open-circuit condition for at least 15 min before the cyclic voltammetry analysis.

Scan rates during cyclic voltammetry ranged from 0.5 to 5 mV s^{-1} and the voltage was scanned between −15 and +15 mV versus open-circuit voltage. Slower scan rates were not employed because the charge passed during slower scan rates led to significant changes in the SOC and thus the open-circuit potential V_0. Conversely, faster scan rates were not employed as the 5 mV s^{-1} scan rate over the 30 mV potential range for the cycle provided a short half-cycle time θ and a nearly linear current–voltage responses (i.e., α substantially greater than 1). Thus, as will be made clear in the next section, the scan rates and cycle durations allowed for a sufficiently broad range in values of $\alpha = RC/\theta$ to be examined.

Tests were conducted using a 1287 Solartron Electrochemical Interface (Solartron Analytical, UK) controlled by Corrware (Scribner Associates Inc., Southern Pines, NC). The cell was maintained at 25 °C; temperature control was provided by a Tenney environment chamber (Model Tenney20, Lunaire, Williamsport, PA).

3. Mathematical relations

This section contains three subsections. First, we provide a means to describe the equilibrium potential consistent with the behavior of intercalation electrodes. Next, analytic expressions are derived for cyclic voltammetry of the cell, and these expressions are used to simulate the experimental data. Last, because the mathematics are quite similar and represent an incremental change to the voltammetry expressions, we present solutions for triangular current sweep chronopotentiometry.

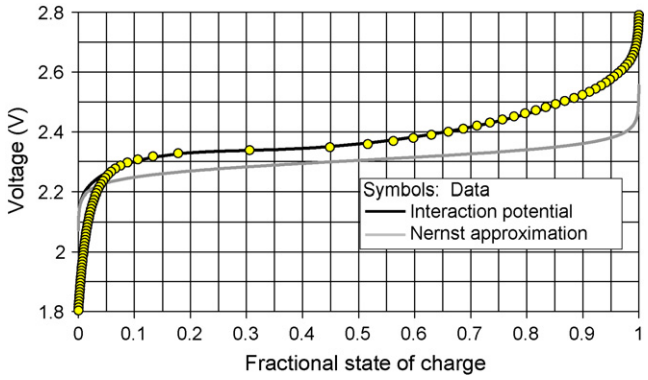

Fig. 2. Open-circuit potential. The interaction potential is provided by Eq. (1), and Eq. (2) corresponds to the depicted Nernst equation.

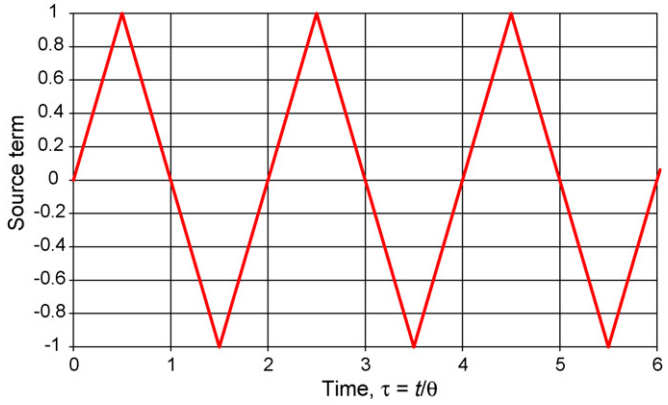

Fig. 3. Source term. For both cyclic current and potential sources ($\tilde{I}$ and $\tilde{V}$, respectively) the plotted source term applies, and the cell is taken to be initially equilibrated; i.e., zero current for a prolonged duration and the cell potential corresponding to the equilibrium value.

3.1. Equilibrium potential

A more complete description of equilibrium relations based on molecular thermodynamics for intercalation electrodes can be found in Refs. [26–28]. By considering repulsion between intercalate species within the capacity-limiting intercalation electrode, we obtain the following relation for the cell potential [27],

$$V_0(\mathrm{SOC}) = U^{\mathrm{o}} - \frac{R_{\mathrm{g}}T}{F}\ln\frac{1-\mathrm{SOC}}{\mathrm{SOC}} + \sum_{j=1,\infty} a_j \mathrm{SOC}^j, \qquad (1)$$

where $j+1$ denotes the number of intercalates involved in the intercalate–intercalate interaction and SOC reflects the fractional state of charge. For our purposes, we truncate the series at $j=6$. The Nernst approximation results from neglecting the summation term used to address lithium–lithium interactions:

$$V_0(\mathrm{SOC}) = U^{\mathrm{o}} - \frac{R_{\mathrm{g}}T}{F}\ln\frac{1-\mathrm{SOC}}{\mathrm{SOC}}. \qquad (2)$$

The coefficients a_j used to generate the interaction potential depicted in Fig. 2 are provided in Table 1. The plot shown in Fig. 2 indicates that interactions between lithium guests in the capacity-limiting electrode are quite weak, as there is less than 1.2 kcal mol^{-1} difference between the Nernst expression and the data at 50% SOC.

Table 1
Interaction coefficients and other values used in Eqs. (1) and (2)

Quantity	Value, V
RT/F	0.02568
U^{o}	2.3044
a_1	0.8889
a_2	−4.4742
a_3	9.4101
a_4	−8.7417
a_5	3.1588
a_6	2.3354×10^{-6}

The temperature corresponds to 25 °C.

3.2. Cyclic voltammetry

The equations governing the circuit depicted in Fig. 1 can be written as

$$I = I_2 + I_3, \qquad V = V_0 + IR + I_3 R_{\mathrm{ct}},$$
$$V = V_0 + IR + \frac{Q}{C}, \qquad I_2 = \frac{\mathrm{d}Q}{\mathrm{d}t}. \qquad (3)$$

A current balance yields the first equation, summing the voltage about loops including the interfacial charge-transfer resistance R_{ct} and capacitance C provides the second and third equations (respectively), and the last equation relates the charge Q on the capacitor in terms of the current passing through it. Substitution can be used to eliminate the currents I_2 and I_3 and the charge Q, which yields a single equation relating the cell current I and potential V:

$$R\frac{\mathrm{d}I}{\mathrm{d}t} + \frac{1}{C}\left(1 + \frac{R}{R_{\mathrm{ct}}}\right) I = \frac{\mathrm{d}V}{\mathrm{d}t} - \frac{1}{R_{\mathrm{ct}}C}(V_0 - V). \qquad (4)$$

It is helpful to nondimensionalize the problem statement with the following definitions:

$$\tau = \frac{t}{\theta}, \qquad \tilde{V} = \frac{V - V_0}{V_{\max} - V_0}, \qquad \tilde{I} = \frac{I}{\nu C},$$
$$\alpha = \frac{RC}{\theta}, \qquad r = \frac{R}{R_{\mathrm{ct}}}.$$

Referring to Fig. 3, we can express the triangular voltage excitation source by means of the Fourier series [29]

$$\tilde{V} = -\frac{8}{\pi^2}\sum_{n=1,3,5,\ldots}^{\infty}\frac{1}{n^2}\cos\left[n\pi\left(\tau + \frac{1}{2}\right)\right].$$

Eq. (4) can now be recast as

$$\alpha\frac{\mathrm{d}\tilde{I}}{\mathrm{d}\tau} + (1+r)\tilde{I} = \frac{1}{2}\left(\frac{r}{\alpha}\tilde{V} + \frac{\mathrm{d}\tilde{V}}{\mathrm{d}\tau}\right) \qquad (5)$$

or

$$\alpha\frac{d\tilde{I}}{d\tau}+(1+r)\tilde{I}=-\frac{r}{\alpha}\frac{4}{\pi^2}\sum_{n=1,3,5,\ldots}^{\infty}\frac{1}{n^2}\cos\left[n\pi\left(\tau+\frac{1}{2}\right)\right]+\frac{4}{\pi}\sum_{n=1,3,5,\ldots}^{\infty}\frac{1}{n}\sin\left[n\pi\left(\tau+\frac{1}{2}\right)\right]. \quad (6)$$

The initial condition corresponds to an equilibrated system, $V=V_0$, and

$$\tilde{I}(0)=0.$$

We have obtained the following solution to these equations:

$$\tilde{I}(\tau)=4\sum_{n=1,3,5,\ldots}^{\infty}\frac{(\alpha^2n^2\pi^2+r+r^2)\{e^{-((1+r)/\alpha)\tau}\cos((1/2)n\pi)-\cos[n\pi(\tau+(1/2))]\}-\alpha n\pi\{e^{-((1+r)/\alpha)\tau}\sin((1/2)n\pi)-\sin[n\pi(\tau+(1/2))]\}}{\alpha n^2\pi^2[\alpha^2n^2\pi^2+(1+r)^2]}. \quad (7)$$

For long times, a uniform and sustained periodic state is obtained, which is of most interest in terms of comparing experiment and theory:

$$\tilde{I}(\text{periodic})=4\sum_{n=1,3,5,\ldots}^{\infty}\frac{\alpha n\pi\sin[n\pi(\tau+(1/2))]-(\alpha^2n^2\pi^2+r+r^2)\cos[n\pi(\tau+(1/2))]}{\alpha n^2\pi^2[\alpha^2n^2\pi^2+(1+r)^2]}. \quad (8)$$

While these equations are cumbersome because of the infinite (albeit convergent) summations, particularly convenient solutions can be obtained by evaluating the summations in Eq. (8) at selected times within the cycle. The current halfway into each cycle ($\tau=1/2$) can be expressed as

$$\tilde{I}\left(\frac{1}{2}\right)=\frac{r+r^2+2\alpha\tanh((1+r)/2\alpha)}{2\alpha(1+r)^2}. \quad (9)$$

We have also obtained analytic solutions at the start and end of each cycle,

$$\tilde{I}(1)=-\tilde{I}(0)=\frac{\operatorname{sech}((1+r)/2\alpha)-1}{(1+r)^2}. \quad (10)$$

We close this section by noting that relative to the previously published capacitor study [1], which involved the simple *RC* circuit (R_{ct} infinite in Fig. 1, corresponding to $r=0$), we recover the same expressions for Eqs. (5)–(10) as $r\to 0$. In addition, these analytic expression are in agreement with those presented by Macdonald [30], after taking into account the differences in the derivation and notation.

3.3. Triangular current sweep chronopotentiometry

Eq. (4) remains as the governing equation, and the current excitation source is depicted in Fig. 3. The appropriate nondimensionalization for the triangular current sweep is

$$\tau=\frac{t}{\theta},\qquad \bar{V}=\frac{V-V_0}{I_{max}R},\qquad \bar{I}=\frac{I}{I_{max}},$$
$$\alpha=\frac{RC}{\theta},\qquad r=\frac{R}{R_{ct}}.$$

Thus, only the dimensionless voltage and current differ from that of the cyclic voltammetry problem, and an overbar is employed to reflect the nondimensionalization of these variables for the triangular current sweep problem. The current excitation source corresponds to

$$\bar{I}=-\frac{8}{\pi^2}\sum_{n=1,3,5,\ldots}^{\infty}\frac{1}{n^2}\cos\left[n\pi\left(\tau+\frac{1}{2}\right)\right],$$

and Eq. (4) can now be written as

$$\alpha\frac{d\bar{V}}{d\tau}+r\bar{V}=(1+r)\bar{I}+\alpha\frac{d\bar{I}}{d\tau}$$

or

$$\alpha\frac{d\bar{V}}{d\tau}+r\bar{V}=-(1+r)\frac{8}{\pi^2}\sum_{n=1,3,5,\ldots}^{\infty}\frac{1}{n^2}\cos\left[n\pi\left(\tau+\frac{1}{2}\right)\right]+\alpha\frac{8}{\pi}\sum_{n=1,3,5,\ldots}^{\infty}\frac{1}{n}\sin\left[n\pi\left(\tau+\frac{1}{2}\right)\right].$$

The initial condition corresponds to a system equilibrated,

$$\bar{V}(0)=0.$$

We can derive solutions quite similar to those for the cyclic voltammetry case:

$$\bar{V}(\tau)=8\sum_{n=1,3,5,\ldots}^{\infty}\frac{(\alpha^2n^2\pi^2+r+r^2)\{e^{-(r/\alpha)\tau}\cos(n\pi)-\cos[n\pi(\tau+(1/2))]\}+\alpha n\pi\{e^{-(r/\alpha)\tau}\sin(n\pi)-\sin[n\pi(\tau+(1/2))]\}}{n^2\pi^2(\alpha^2n^2\pi^2+r^2)}.$$

The stationary state (uniform and sustained periodic state) corresponds to

$$\bar{V}(\text{periodic}) = -8 \sum_{n=1,3,5,\ldots}^{\infty} \frac{\begin{array}{l}\alpha n\pi \sin[n\pi(\tau + (1/2))] \\ +(\alpha^2 n^2\pi^2 + r + r^2)\cos[n\pi(\tau + (1/2))]\end{array}}{n^2\pi^2(\alpha^2 n^2\pi^2 + r^2)}.$$

As in the case of cyclic voltammetry, the infinite summations can be recast as simple expressions at various points within the cycle,

$$\begin{aligned} \bar{V}(1) &= -\bar{V}(0) = \frac{2\alpha}{r^2}\left[1 - \operatorname{sech}\left(\frac{r}{2\alpha}\right)\right] \\ \bar{V}\left(\frac{1}{2}\right) &= \frac{r + r^2 - 2\alpha\tanh(r/2\alpha)}{r^2} \end{aligned} \quad . \tag{11}$$

4. Results

The variation in the current response to the voltage excitation is represented by the plots shown in Figs. 4 and 5. The two dimensionless groups that govern the problem, $\alpha = RC/\theta$ and $r = R/R_{ct}$, are varied to examine their influence. For $r = 0$, the previously published expressions and plots are obtained [8], which have been helpful in describing the performance of supercapacitors. As r is decreased, reflecting increased interfacial resistance R_{ct}, the dimensionless current $I/\nu C$ is deceased, and the dimensionless voltammogram exhibits increased hysteresis. Conversely, decreasing α leads to increasing dimensionless currents $I/\nu C$ and more ohmic behavior; i.e., increasing linearity in the voltammogram and reduced hysteresis. Increasing hysteresis is reflected by a larger magnitude in the current $I/\nu C$ at the potential $(V - V_0)/(V_{max} - V_0) = 0$.

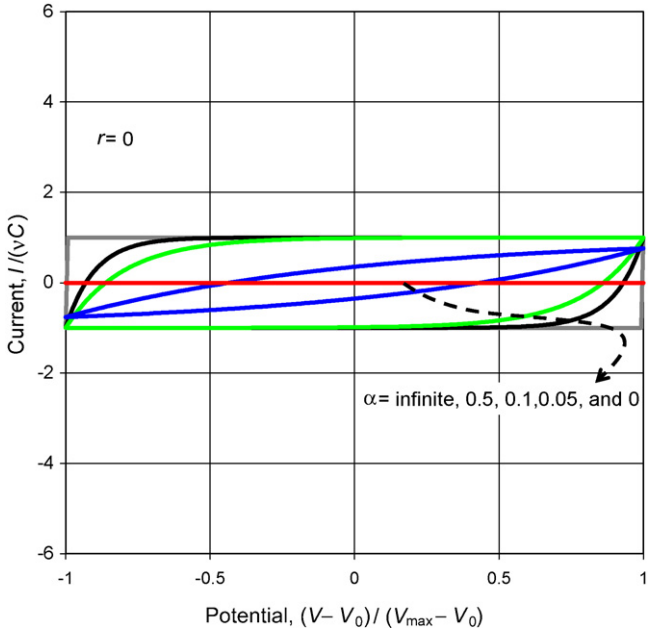

Fig. 4. Cyclic voltammogram for infinite resistance R_{ct}. In this case, a series resistor–capacitor circuit prevails (cf. Fig. 1), and the analytic solution presented in Ref. [8] applies.

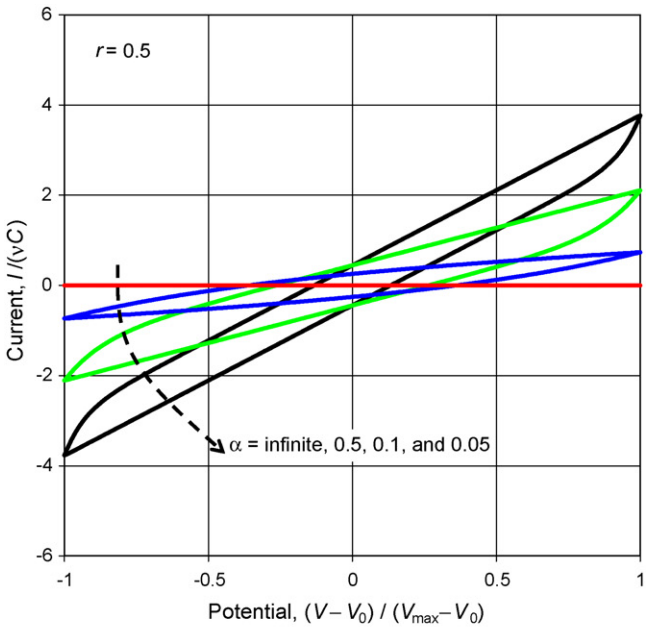

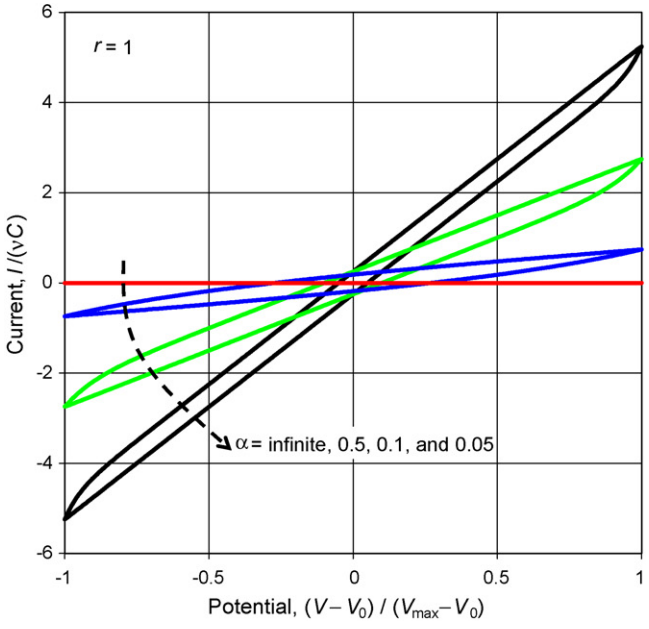

Fig. 5. Influence of $\alpha = RC/\theta$ and $r = R/R_{ct}$ on the system response.

The series of plots depicted in Figs. 6–9 provides comparisons between the analytic stationary-state voltammogram (Eq. (8)) and experimental data. In general, very good agreement was obtained, as the salient features of the plotted experimental voltammograms are reflected by the accompanying calculations. As the scan rate is increased, less hysteresis is displayed, and the current–voltage relation becomes linear. Because the current is scaled with the scan rate, the dimensionless current $I/\nu C$ declines with increasing scan rate. As the SOC increases, the hysteresis increases, which is reflected by an increase in R_{ct} and a decrease in C.

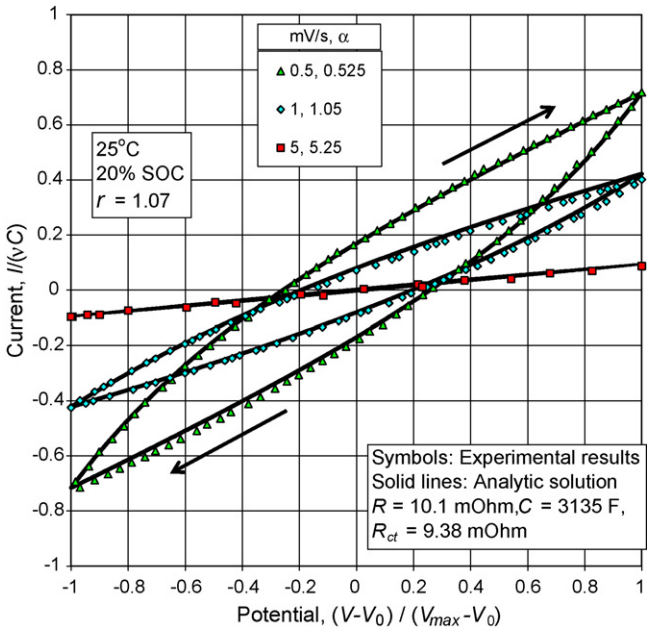

Fig. 6. Experiment–theory comparison at 20% state of charge.

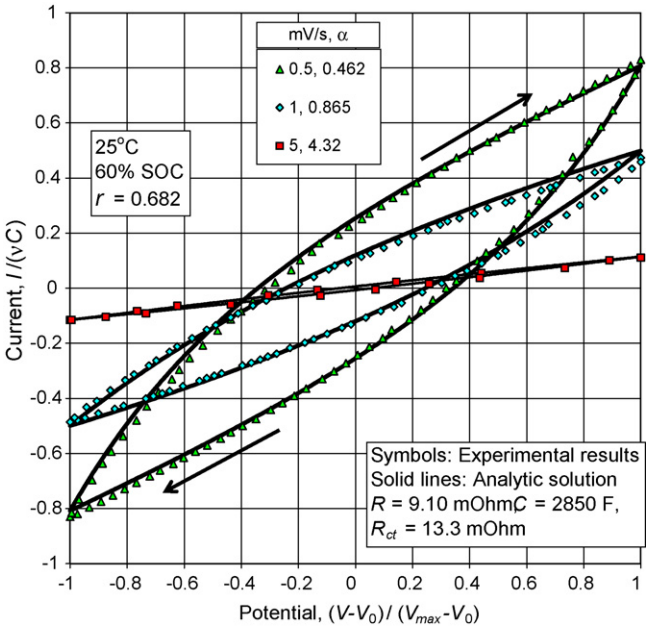

Fig. 8. Experiment–theory comparison at 60% state of charge.

The trend in the parameters R, R_{ct}, and C with variations in SOC is illustrated in Fig. 10. The parameters are effectively constant for the constant-voltage portion of the open-circuit potential curve, and they change in a substantially monotonic manner for SOC values above 50% SOC.

5. Summary and open questions

For cyclic voltammetry and triangular current sweep chronopotentiometry, a uniform and sustained periodic state is obtained for batteries, which is of interest in terms of comparing experiment and theory, and which admits a convenient analytic solution that facilitates parameter extraction. Particularly simple expressions result for the response at the start, end, and mid-point of the cycle in the periodic (stationary) state. This work is an extension of our earlier analysis of supercapacitor electrodes [8].

The parameters governing the cell impedance are constant over the constant-voltage portion of the cell potential, and vary monotonically throughout the sloping portion of the open-circuit potential (i.e., above approximately 50% state of charge; cf. Fig. 10).

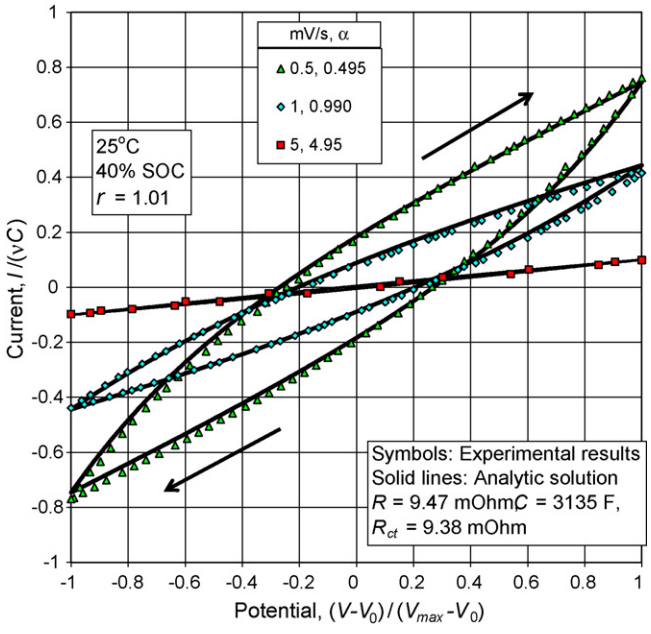

Fig. 7. Experiment–theory comparison at 40% state of charge.

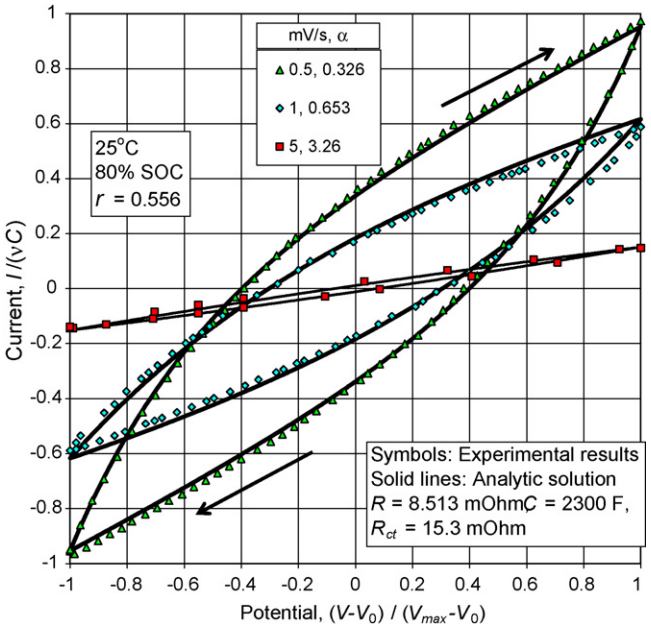

Fig. 9. Experiment–theory comparison at 80% state of charge.

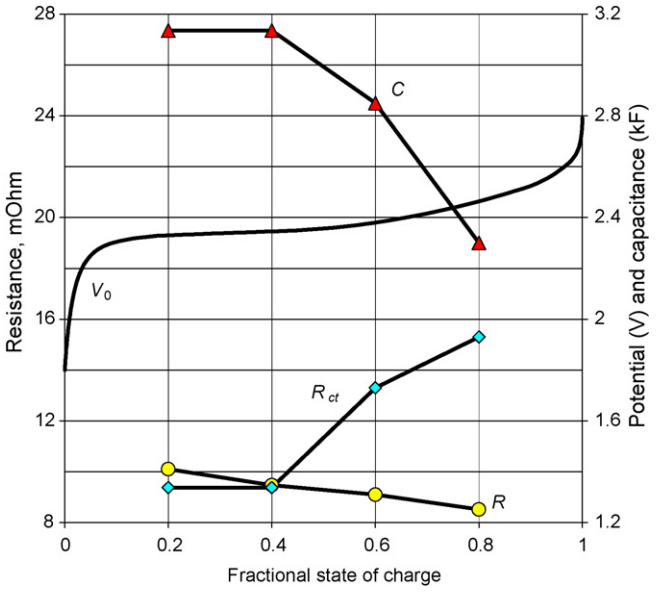

Fig. 10. Summary of experiment–theory comparisons.

In addition to not addressing microscopic phenomena within the cell that provides a more comprehensive understanding of the system, the primary short coming of the method described in this work is the lack of low-frequency information. The analytic expressions are derived assuming the open-circuit potential V_0 is constant as the potential is scanned over a small range (30 mV in this work). It is clear from the inspection of Fig. 2 that the small variations in potential can lead to large variations in SOC, particularly for the flat region of the curve, and this limits the use of slow scan rates. A richer analysis would include SOC variations and the influence of diffusion processes in a more detailed manner, perhaps by incorporating a Warburg impedance element as a starting point [31]. Because the SOC would change over the course of the cycle, it is doubtful that useful analytic formulae can be derived for this case; the resulting numerical model, however, should be easily integrated.

While the parameter analysis presented in this work does address SOC variations between experiments (cf. Fig. 10), the circuit parameters will also change with temperature, and we have only investigated room temperature variations in this work. This discussion highlights the need to identify parameter values over a range of experimental conditions (particularly over temperature and SOC ranges); the very simple expressions we derive (Eqs. (9) and (10) for cyclic voltammetry and Eqs. (11) for triangular current sweep chronopotentiometry) should prove helpful for extracting parameters over a broad range of temperatures.

In closing, we note that the ability of the simple circuit depicted in Fig. 1 to accurately represent the experimental cyclic-voltammetry data implies that the equivalent circuit can be used to represent this class of titanate-based cells and that the equivalent circuit should work well for the purposes of constructing model-based state estimators [1–5] for hybrid-electric vehicle applications or other applications wherein the state of the energy storage device must be ascertained.

References

[1] S. Pillar, M. Perrin, A. Jossen, J. Power Sources 96 (2001) 113.
[2] M.W. Verbrugge, E.D. Tate, J. Power Sources 126 (2004) 236.
[3] M.W. Verbrugge, P. Liu, S. Soukiazian, J. Power Sources 141 (2005) 369.
[4] M.W. Verbrugge, D. Frisch, B. Koch, J. Electrochem. Soc. 152 (2005) A333.
[5] M.W. Verbrugge, B.J. Koch, J. Electrochem. Soc. 153 (2006) A187.
[6] http://www.uscar.org/consortia&teams/consortiahomepages/consusabc.htm.
[7] A.J. Bard, L.R. Faulkner, Electrochemical Methods, Wiley, New York, 1980.
[8] M.W. Verbrugge, P. Liu, J. Electrochem. Soc. 153 (2006) A1237.
[9] A. Gelb (Ed.), Applied Optimal Estimation, M.I.T. Press, Cambridge, MA, 1974.
[10] B.D.O. Anderson, J.B. Moore, Optimal Filtering, Prentice-Hall, Englewood Cliffs, NJ, 1979.
[11] P.S. Maybeck, Stochastic Models, Estimation and Control, vol. 141-1 of Mathematics in Science and Engineering, Academic Press, 1979.
[12] B. Widrow, S.D. Stearn, Adaptive Signal Processing, Prentice-Hall, Englewood Cliffs, NJ, 1985.
[13] W.L. Brogan, Modern Control Theory, second ed., Prentice-Hall, Englewood Cliffs, NJ, 1985.
[14] L. Ljnug, T. Söderström, Theory and Practice of Recursive Identification, MIT Press, 1986.
[15] M.G. Bellanger, Adaptive Digital Filters and Signal Analysis, Marcel Dekker, New York, NY, 1987.
[16] K.J. Åström, B. Wittenmark, Adaptive Control, Addison-Wesley, 1989.
[17] R. Kulhavý, Recursive Nonlinear Estimation. A Geometric Approach, Springer, London, 1996.
[18] Y. Zheng, Z. Lin, IEEE Trans. Circuits Syst.—II: Anal. Digital Signal Process. 50 (2003) 602.
[19] S. Sathyanarayana, S. Venugopalan, M.L. Gopikanth, J. Appl. Echem. 9 (1979) 369.
[20] M.L. Gopikanth, S. Sathyanarayana, J. Appl. Echem. 9 (1979) 369.
[21] M.S. Suresh, S. Sathyanarayana, J. Power Sources 37 (1992) 335.
[22] S. Rodrigues, N. Munichandraiah, A.K. Shukla, J. Power Sources 87 (2000) 12.
[23] V.V. Viswanathan, A.J. Salkind, J.J. Kelley, J.B. Ockerman, J. Appl. Echem. 25 (1995) 716.
[24] V.V. Viswanathan, A.J. Salkind, J.J. Kelley, J.B. Ockerman, J. Appl. Echem. 25 (1995) 729.
[25] F. Huet, J. Power Sources 70 (1998) 59.
[26] M.W. Verbrugge, B.J. Koch, J. Electrochem. Soc. 146 (1999) 833.
[27] M.W. Verbrugge, R.S. Conell, J. Electrochem. Soc. 149 (2002) A45.
[28] M.W. Verbrugge, B.J. Koch, J. Electrochem. Soc. 143 (1996) 600.
[29] W.H. Beyer (Ed.), Standard Mathematical Tables, 24th ed., CRC Press, Cleveland, OH, 1976, p. 406.
[30] D.D. Macdonald, J. Electrochem. Soc. 125 (1978) 1443.
[31] E. Barsoukov, J.R. Macdonald (Eds.), Impedance Spectroscopy. Theory, Experiment, and Applications, second ed., Wiley, 2005.